www.vbripress.com, www.amlett.com, DOI: 10.5185/amlett.2012.3325 Published online by the VBRI press in 2012

Microstructure and dielectric relaxation of BT and ST doped $Ba(Fe_{0.5}Nb_{0.5})O_3$ ceramics for sensor applications

N. K. Singh[1*], Pritam Kumar[1], Chandra Prakash[2]

[1]*University Department of Physics, V. K. S. University, Ara 802 301 Bihar, India*
[2]*Directorate of IE & IPR, DRDO, DRDO Bhawan, New Delhi 110011, India*

[*]Corresponding author. Tel: (+91) 9431850564; E-mail: singh_nk_phy27@yahoo.com

Received: 12 March 2012, Revised: 26 April 2012 and Accepted: 28 April 2012

ABSTRACT

Recently a new wave of interest has risen on complex perovskite structure due to their wide use in fabrication of multilayer ceramic capacitors, electrostrictive actuators, and electromechanical transducers. The polycrystalline ceramics of $Ba(Fe_{0.5}Nb_{0.5})O_3$ (BFN) and its solid solutions $0.89Ba(Fe_{0.5}Nb_{0.5})O_3$-$0.11BaTiO_3$ (BFN-BT11) and $0.89Ba(Fe_{0.5}Nb_{0.5})O_3$-$0.11SrTiO_3$ (BFN-ST11) were fabricated by a solid-state reaction Method. Processing parameters such as calcination temperature, sintering temperature and sintering durations were optimized to get best dielectric properties. It was found that the above ceramics sintered at 1250°C for 6 hours exhibited maximum density and uniform microstructure. X-ray diffraction studies of the compound showed the formation of single-phase monoclinic crystal structure at room temperature. Surface morphology of the compounds was studied by Scanning electron microscope (SEM). The effects of $BaTiO_3$ and $SrTiO_3$ substitution on the structure and on the electrical and ferroelectric properties of $Ba(Fe_{0.5}Nb_{0.5})O_3$ samples have been studied by performing x-ray diffraction and dielectric measurements. The electrical properties of the samples were investigated in a frequency range of 100 Hz - 1 MHz and temperature range of 30-350 °C using complex impedance spectroscopic technique. The frequency-dependent electrical data are also analyzed in the framework of conductivity and impedance formalisms.

Keywords: Perovskite oxides; dielectric constant; electrical properties; scanning electron micrographs.

N. K. Singh obtained his M.Sc. degree in physics from Bihar University, Muzaffarpur, India in 1969 and Ph.D. in 1984 from Patna University, Patna. He is Professor and Head, University Department of Physics, V.K.S. University, Ara (India). He is the life member of different academic and Research Societies of India and abroad. He is a member of the Editorial Board of National Journal "ARJP". More than eighteen students have completed their Ph.D. degrees, under his guidance. He has published more than 72 research papers in peer reviewed journals of the world. He was a U.G.C. Visiting Associate at I.I.T. Kharagpur, India during 2001-2003. In span of 27 years of his research career, he has remained engaged in the preparation of fine ceramics, ferroelectric piezoelectric and non-Lead based materials. Presently, he is Principal Investigator of Major Research Project sponsored by DRDO, New Delhi and is engaged in synthesis and characterization of Lead free ferroelectric-piezoelectric systems for sensor applications.

Pritam Kumar obtained M.Sc. degree in physics from T. M. Bhagalpur University, Bhagalpur, India in 2005. He has submitted his Ph.D. Thesis in University in 2012. Presently, he is working as JRF/SRF in Major Research Project sponsored by DRDO, New Delhi since 2009 at V.K.S. University, Department of Physics. During his research career, he involved in the preparation of fine ceramics, ferroelectric, piezoelectric and non-lead based materials.

Chandra Prakash is presently Associate Director, Directorate of Extramural Research & Intellectual Property Rights, DRDO, Delhi, India. Earlier, he was Head of Electroceramics Group at Solid State Physics Laboratory, Delhi. He received his Ph.D. from Delhi University. He is co-recipient of DRDO Technology awards for the years 1988, 1995 and 2002. He received MRSI Medal for the year 2012. He is Chairman of Delhi Chapter of Materials Research Society of India (MRSI). He was Visiting Scientist at Penn State University, USA during 1994-95. He has more than 175 research publications in reputed journals with more than 900 Citations and h-index 17. He has 2 patents. His current interests are focused on ferroelectrics, piezoelectrics, microwave dielectrics, ferrites, composites etc.

Introduction

A sudden change in polarization with respect to electric field is known as spontaneous polarization. The material which has spontaneous polarization (P_s) and reverses it by the application of electric field is called as ferroelectric materials. The ferroelectricity was first discovered by Valasek in Rochelle salt ($KNaC_4H_4O_6.4H_2O$) in 1921. Later on a large number of ferroelectrics like $BaTiO_3$, KH_2PO_4, $PbNb_2O_6$, $KNbO_3$, $PbTiO_3$ etc. have been discovered. Ferroelectrics are the key materials in microelectronics. Their excellent dielectric properties make them suitable for electric components such as tunable capacitors and memory cells.

A large number of perovskite materials exhibit a ferroelectric behavior depending on the composition; these materials can be divided in two classes: classical ferroelectrics or relaxor ferroelectrics. Classical ferroelectrics are characterized by square hystereris loop, large coercive fields, large remnant polarization (P_R) and spontaneous polarization (P_s). Polarization vanishes at transition temperature (T_c). The vanishing is continuous for second order transition while discontinuous for the first order transition. The transition from paraelectric to ferroelectric state is sharp in the dielectric response. The temperature dependence of ε_T obeys Curie-Weiss law just above T_c and thermal hysteresis is observed in the dielectric response, whereas relaxor ferroelectrics are characterized by slim hysteresis loop, small coercive fields, small remnant polarization (P_R) and spontaneous polarization (P_s). Polarization does not vanish at transition temperature but vanishes at higher temperature called Burns temperature, T_n. Relaxor ferroelectrics are characterized by diffused phase transition. The dielectric permittivity of the relaxor attains a maximum value at the temperature T_{max} for particular frequency. As the frequency increases, T_{max} increases to higher temperature. The temperature dependence of ε_T does obey Curie-Weiss law just above T_{max} but obeys beyond T_n ($T_n > T_{max}$) **[1]**. Relaxor materials are of great interest both for device applications and in the fundamental understanding of ferroelectric systems **[2, 3]**. The relaxor ferroelectric materials exhibit a large range of interesting properties related to their complex order/disorder nanostructures. The main characteristic of this material group is the extraordinary large, diffuse and frequency dispersive maximum in the temperature (T_m) dependence of dielectric permittivity (ε_m). This typical phenomenon is caused by the presence of polar nano-regions (PNR) into the structure **[4].**

The alternating current impedance spectroscopy (ACIS) is a very convenient and powerful experimental technique that enables us to correlate the electrical properties of a material with its microstructure, and also helps to analyze and separate the contributions, from various components (i.e., through grains, grain boundary, interfaces, etc.) of polycrystalline materials in the wide frequency range. ACIS allows the measurement of capacitance (C) and the loss tangent (tanδ) or real and imaginary impedance over a wide frequency range. From the measured C and tanδ, four complex dielectric functions can be computed impedance (Z^*), permittivity (ε^*), electric modulus (M^*) and admittance (Y^*) to explain the dielectric behavior and electrical conductivity of a wide range of materials. If the current I and voltage V are considered to have a time variation of $e^{i\omega t}$ the quantity V/I is a complex number with no time dependence and is called the complex impedance Z^*, the real part (Z') may be interpreted as resistance and the imaginary part (Z'') may be interpreted as capacitance with-

$$Z^{-1} = \frac{1}{R} + j\omega C \text{ where } j = \sqrt{-1},$$

C is the capacitance and ω is the angular frequency of the ac field **[5]**. Impedance analysis basically involves the display of the impedance data in different formalism and provides us the maximum possible information about the materials. The display of impedance data in the complex plane plot appears in the form of a succession of semicircles attributed to relaxation phenomena with different time constants due to the contribution of grain (bulk), grain boundary and interface/polarization in a polycrystalline material**.** Hence, the contributions to the overall electrical property by various components in the material are separated out easily.

Complex perovskite oxides are very promising for electroceramic applications and many researchers have shown considerable interest in the dielectric properties of these compounds. Materials having a diffuse phase transition (relaxors) have attracted the most attention due to their broad maximum in the temperature dependence of their dielectric constant **[6, 7]**.

Perovskite type complex ceramics with general formula $A(B'B'')O_3$ exhibiting high dielectric constant ($\varepsilon' > 10^3$) are of enormous importance to the electronic and/or microelectronic industries due to their wide applications as industrial capacitors, sensors, actuators, memory devices, power transmission devices, high energy storage devices, etc. It is observed from the literature that a complex perovskite oxides such as $Ba(Fe_{1/2}Nb_{1/2})O_3$ **[8-15]**, $Ba(Bi_{1/2}Nb_{1/2})O_3$ **[16, 17]**, $Ba(Al_{1/2}Nb_{1/2})O_3$ **[18, 19]**, etc., exhibit a relaxor behavior by showing very attractive dielectric and electric properties over a wide range of temperatures.

The high value of dielectric constant over a very wide range of temperature interval is due to disorder in the distribution of B-site ions in the perovskite unit cell. Various relaxation processes seem to coexist in real perovskite crystals or ceramics, which contain number of different energy barriers due to point defects appearing during technological process. Therefore, the departure of the response from the ideal Debye model in the solid-state samples, resulting from the interaction between the dipoles, cannot be disregarded **[20, 21]**.

$BaTiO_3$ and $SrTiO_3$ based dielectrics are more focused in research field, due to its not detrimental to the environment both in synthesis and its application. The compositions of the majority dielectric materials used for ceramic capacitors are based on barium/strontium titanate **[22-24]**. In the present work, BFN and its solid solution BFN-BT11 and BFN-ST11 was fabricated by a solid-state reaction method and their dielectric characteristics are evaluated in broad temperature and frequency ranges.

Experimental

Ceramic powders of $Ba(Fe_{0.5}Nb_{0.5})O_3$ (BFN) and its solid solutions $0.89Ba(Fe_{0.5}Nb_{0.5})O_3$-$0.11BaTiO_3$ (BFN-BT11) and $0.89Ba(Fe_{0.5}Nb_{0.5})O_3$-$0.11SrTiO_3$ (BFN-ST11) was fabricated by a high temperature solid-state reaction technique using carbonates and oxides; $BaCO_3$ (high-purity ≥99%, M/S-Merck Pvt. Ltd.), $SrCO_3$ (high-purity ≥98%, M/S-Loba Chemie Pvt. Ltd.), Fe_2O_3, Nb_2O_5 (high-purity ≥98%, M/S-Loba Chemie Pvt. Ltd.) and TiO_2 (high-purity ≥99%, M/S-Merck Pvt. Ltd.). The above ingredients (carbonates & oxide) were mixed thoroughly in a desired stoichiometry using agate mortar and pestle, first in air atmosphere for 2 h and then in acetone medium for 6 h. The mixture was calcined at an optimized temperature/time (1200°C, 8 h). A small amount of polyvinyl alcohol (PVA) was added to the calcined powder for fabrication of pellets. The calcined fine powder was cold pressed into cylindrical pellets of 10 mm diameter and 1-2 mm of thickness by applying uniaxial pressure of $5x10^6$ N/m^2. The pellets were subsequently sintered at an optimized temperature/time (1250°C, 6 h). A preliminary structural study was carried out using an X-ray diffraction (XRD) technique with an X-ray powder diffractometer (Rigaku Miniflex, Japan) for the confirmation of formation of the compound. CuKα radiation (λ= 1.5405 Å) was employed in the wide range of Bragg angles (20°≤ θ≤80°) at a scan speed of 2° min^{-1}. For electrical measurement of the compound, air drying silver paint was applied on both the flat faces of the sample. Impedance parameters (Z), Phase angle (θ), Capacitance (Cp) and loss tangent (D) were measured as a function of frequency (100Hz-1MHz) at different temperatures (30-350°C) using a computer-controlled LCR meter (HIOKI 3235-50 LCR Hi Tester, Japan) in conjunction with a laboratory-made sample holder and heating arrangement with an AC signal (1.2 V).

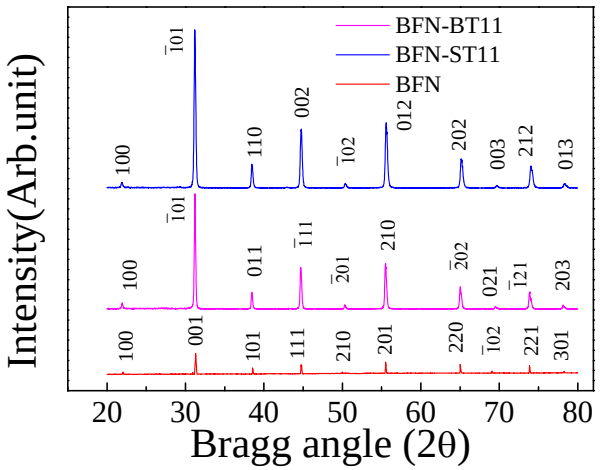

Fig. 1. XRD patterns of BFN, BFN-11BT and BFN-11ST ceramics at room temperature.

Results and discussion

Structural and microstructural analysis

The X-ray powder diffraction patterns **(Fig. 1)** of BFN, BFN-BT11 and BFN-ST11 samples were recorded at room temperature over a range of Bragg angles (20°≤2θ≤80°) on a high accuracy Diffractometer Rigaku Miniflux II using the CuKα radiation (1.39217 Å) of a rotating anode generator of 25 KW. From the measurement taken data were fitted with a computer program (POWDMULT) **[25]**.

Table 1. Comparison of some observed (obs) and calculated (cal) d-values (in Å) of some reflections of BFN, BFN-BT11, and BFN-ST11 compounds at room temperature with intensity ratio I/I_0 . The estimated error in d is ± 0.0001 Å.

(hkl)	BFN d (Å)	(hkl)	BFN-11BT d (Å)	(hkl)	BFN-11ST d (Å)
(100)	[o] 4.0337 (17)	(100)	[o] 4.0477 (6)	(100)	[o] 4.0550 (4)
	[c] 4.0337		[c] 4.0477		[c] 4.0550
(001)	[o] 2.8553 (100)	$(\bar{1}01)$	[o] 2.8643 (100)	$(\bar{1}01)$	[o] 2.8660 (100)
	[c] 2.8553		[c] 2.8643		[c] 2.8660
(101)	[o] 2.3410 (43)	(011)	[o] 2.3375 (15)	(110)	[o] 2.3375 (16)
	[c] 2.3410		[c] 2.3375		[c] 2.3375
(111)	[o] 2.0213 (55)	$(\bar{1}11)$	[o] 2.0264 (37)	(002)	[o] 2.0221 (38)
	[c] 2.0213		[c] 2.0264		[c] 2.0221
(210)	[o] 1.8181 (26)	$(\bar{2}01)$	[o] 1.8111 (4)	$(\bar{1}02)$	[o] 1.8104 (3)
	[c] 1.8226		[c] 1.8123		[c] 1.8109
(201)	[o] 1.6581 (66)	(210)	[o] 1.6543 (40)	(012)	[o] 1.6515 (42)
	[c] 1.6537		[c] 1.6535		[c] 1.6512
(220)	[o] 1.4331 (56)	$(\bar{2}02)$	[o] 1.4328 (20)	(202)	[o] 1.4304 (19)
	[c] 1.4331		[c] 1.4321		[c] 1.4305
$(\bar{1}02)$	[o] 1.3578 (30)	(021)	[o] 1.3510 (3)	(003)	[o] 1.3473 (2)
	[c] 1.3573		[c] 1.3510		[c] 1.3481
(221)	[o] 1.2816 (52)	$(\bar{1}21)$	[o] 1.2820 (15)	(212)	[o] 1.2796 (14)
	[c] 1.2800		[c] 1.2821		[c] 1.2794
(301)	[o] 1.2175(29)	(203)	[o] 1.1175 (4)	(013)	[o] 1.2197 (3)
	[c] 1.2154		[c] 1.1180		[c] 1.2195

Table 2. Structural data of BFN, BFN-BT11, and BFN-ST11 compounds.

Sample	Structure	a	b	c	β (in degree)	V
BFN	Monoclinic	4.0337 Å	4.0734 Å	2.8553 Å	90.12	46.92
BFN-11BT	Monoclinic	4.0477 Å	4.0357Å	2.8674Å	90.25	46.84
BFN-11ST	Monoclinic	4.0550 Å	4.0443Å	2.8643Å	90.10	46.91

A good agreement between the observed and calculated d-values (**Table 1**), suggests the correctness of the selection of crystal system and cell parameters. All the peaks were found to match very well with the experimental data. The cell parameters with cell volume are shown in **Table 2**. X-ray diffraction confirms that BFN, BFN-BT11 and BFN-ST11 ceramics is single phase with monoclinic structure.

The scanning electron micrograph of the samples was recorded by FEI Quanta 200 equipment to check proper compactness of the sample is shown in **Fig. 2**. The nature of the micrographs exhibits the polycrystalline texture of the material having highly distinctive and compact rectangular/cubical grain distributions. The grain size of the pellet sample was found to be in the range of 2-3 μm. Grains are distributed randomly in the samples surface. For the solid solution (BFN-BT11 and BFN-ST11 ceramics), the grain sizes are reduced to favor the matter transport mechanism during the sintering process. When the powders are submitted to the sintering process performed at 1250°C for 5 h, the movement of atoms or molecules is driven by differences in curvature between the particles in contact. In order to reduce surface free energy, atoms supposedly move from particles with smaller radius to those with larger radius [**20**]. Particularly, for the BFN, BFN-BT11 and BFN-ST11 ceramics, it is possible that the matter transport between several aggregated particles and the high

anisotropy in the grain boundary energies induced the formation of compact and irregular particles.

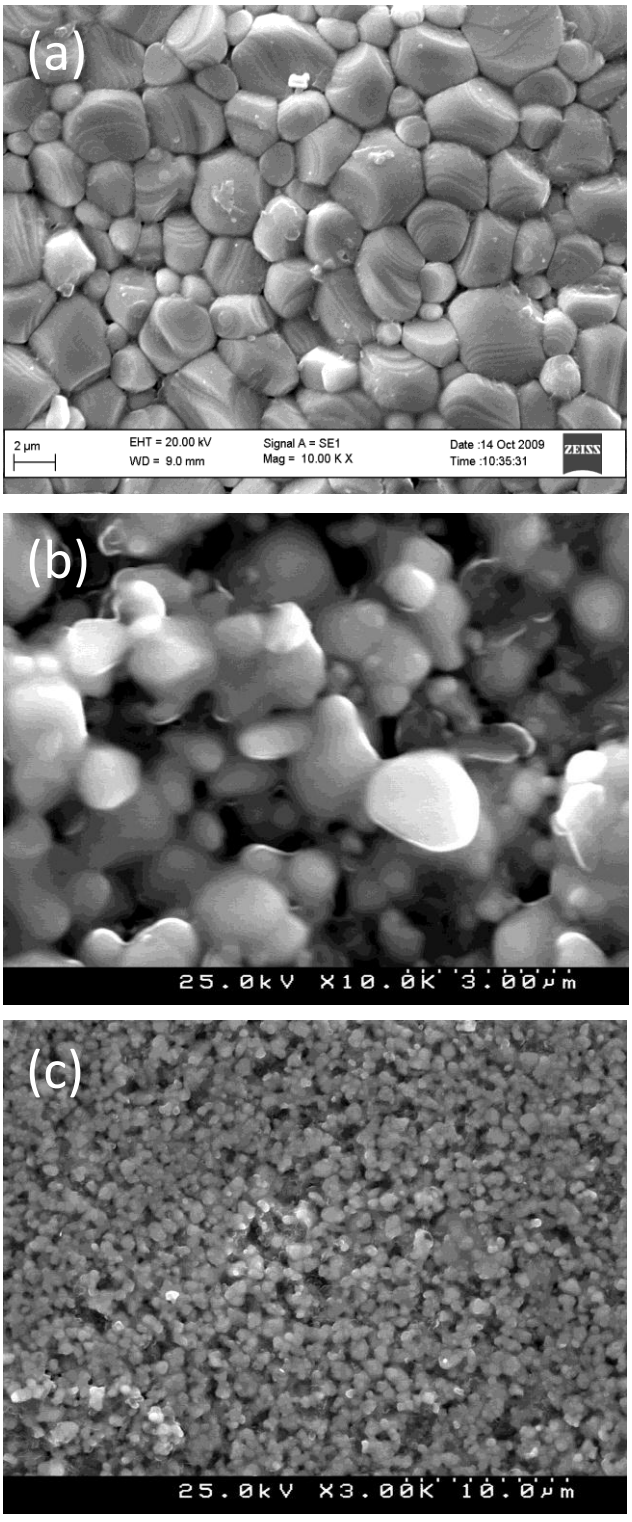

Fig. 2. SEM micrographs of (a) BFN, (b) BFN-BT11 and (c) BFN-ST11, ceramics at room temperature.

Dielectric studies

The frequency dependence of dielectric constant (ε′) and tangent loss (tanδ) for BFN, BFN-BT11 and BFN-ST11 ceramics at various temperatures is shown in **Fig. 3** and **Fig. 4** respectively. It can be seen that ε′ and tanδ decreases rapidly with increasing frequency in the lower frequency range and appears to attain a saturation limit for frequencies > 10^3 kHz.

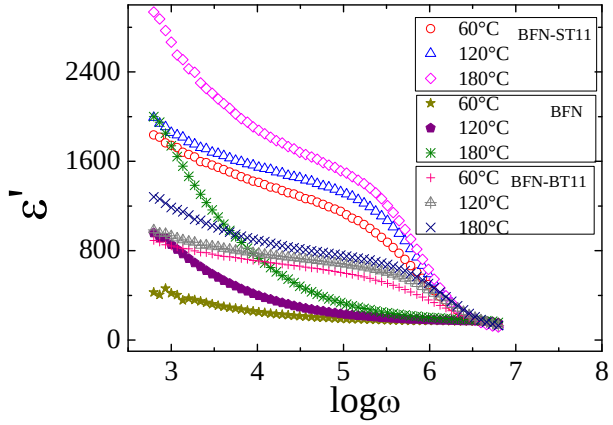

Fig. 3. Logarithmic angular frequency dependence of dielectric constant (ε′) of BFN, BFN-BT11 and BFN-ST11, ceramics at selected temperatures.

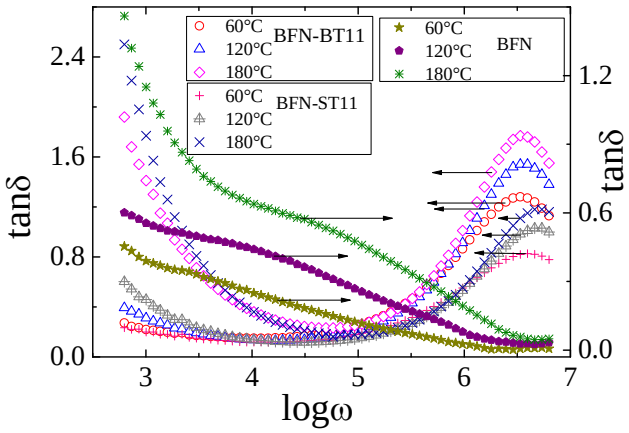

Fig. 4. Tangent loss (tanδ) of BFN, BFN-11BT and BFN-11ST, as a function of logarithmic angular frequency at selected temperatures.

Variations in the dielectric constant and loss tangent may be attributed to different types of polarizations viz., ionic, electronic, dipolar and interfacial or space charge which arise at different stages of materials response to varying temperature and frequency of the applied alternating field. Each mechanism viz. interfacial polarization, dipole polarization, ionic polarization and electronic polarization involves a short range displacement of charges and contributes to the total polarization and then to the dielectric constant of the material **[26]**. The observed dielectric response is similar to the other compounds of the family studied by our groups in their ceramic form **[27-33]**. In BFN-BT11 and BFN-ST11 ceramics, the tanδ peaks were observed which shift towards the higher frequency region (with rise in temperature). This type of feature suggests the presence of dielectric relaxation in the compound **[34, 35]**.

The variation of dielectric constant (ε′) and tangent loss (tanδ) of BFN, BFN-BT11 and BFN-ST11 ceramics measured as a function of temperature at different frequencies is shown in **Fig. 5** and **Fig. 6** respectively. In pure BFN, the relative dielectric constant increases linearly with rise in temperature at different frequencies. However,

no phase transition was observed in the experimental temperature range. But in BFN-BT11 and BFN-ST11 ceramics, it is observed that the dielectric constant increases gradually with an increase in temperature up to transition temperature (Tc) and then decreases. Peaks of the curves i.e. the maximum dielectric constant is decreases with increasing frequency. The region around the dielectric peak is apparently broadened. The broadening or diffuseness of peak occurs mainly due to compositional fluctuation and/or substitution disordering in the arrangement of cations in one or more crystallographic sites of above ceramics. From **Fig. 6**, it is clear that in the low temperature region, tanδ is almost constant up to a certain temperature and then increases faster up to a highest temperature (~350°C) in above ceramics.

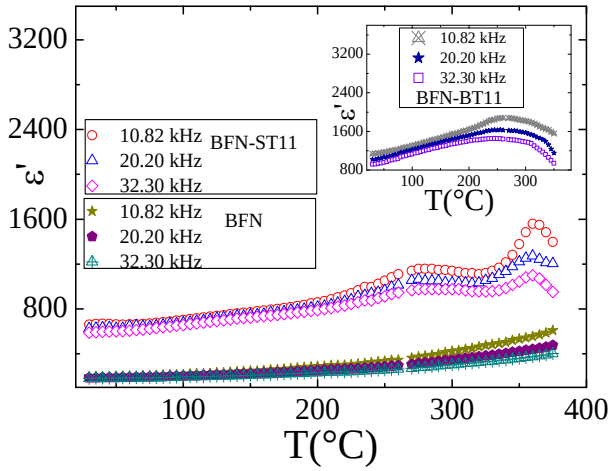

Fig. 5. dielectric constant (ε′) of BFN, BFN-BT11 and BFN-ST11, ceramics as a function of temperature at selected frequencies.

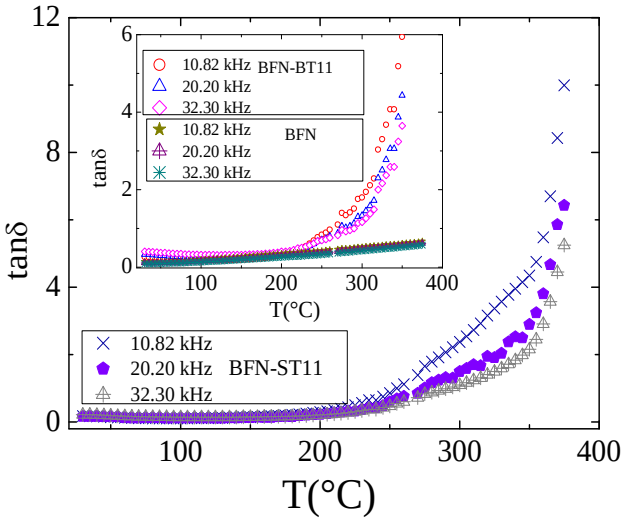

Fig. 6. Tangent loss (tanδ) of BFN, BFN-BT11 and BFN-ST11, ceramics as a function of temperature at selected frequencies.

Electric modulus formalism

The variation of M' and M″ of BFN, BFN-BT11 and BFN-ST11 ceramics measured as a function of frequency at different temperatures is shown in **Fig. 7** and **Fig. 8** respectively. Complex modulus formalism is a very important and convenient tool to determine, analyze and interpret the dynamical aspects of electrical transport phenomena, i.e., parameters such as carrier/ion hopping rate, conductivity relaxation time, etc. It provides an insight into the electrical processes characterized by the smallest capacitance of the materials. The value of M' increases with the increase in frequency and decreases with rise in temperature and it shows a dispersion tending towards M_∞ (the asymptotic value of M′ at higher frequencies). It may be contributed to the conduction phenomena due to short range mobility of charge carriers. The nature of the variation indicates that the electrical properties of the materials arise due to the bulk (intragrain). This implies the lack of a restoring force for flow of charge under the influence of a steady electric field **[36]**.

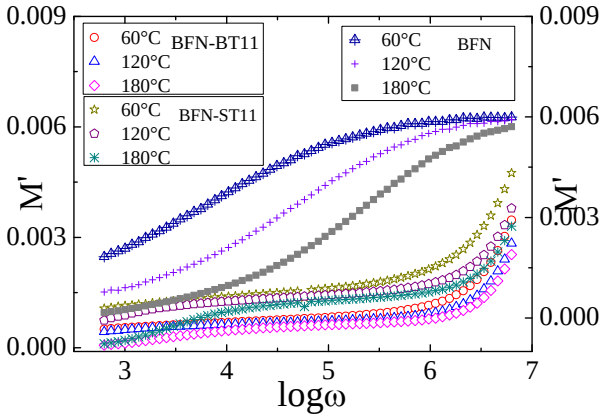

Fig. 7. M' of BFN, BFN-BT11 and BFN-ST11, ceramics as a function of logarithmic angular frequency at various temperatures.

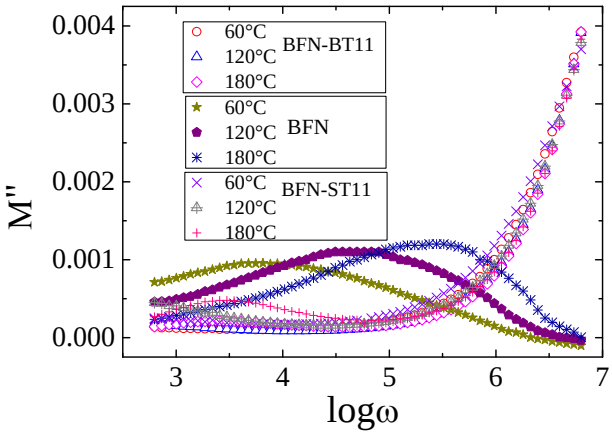

Fig. 8. Logarithmic angular frequency dependence of M″ for BFN, BFN-BT11 and BFN-ST11, ceramics at various temperatures.

From **Fig. 8**, the asymmetric modulus peaks shift towards higher frequency side, indicating correlation between motions of mobile ion charges. The asymmetry in peak broadening shows the spread of relaxation times with different time constants, and hence relaxation is of non-Debye type. The existence of low-frequency peaks suggests that the ions can move over long distances, whereas high-frequency peaks suggest confinement of ions in their potential well. The nature of modulus spectrum confirms the existence of the hopping mechanism in the electrical conduction of the material.

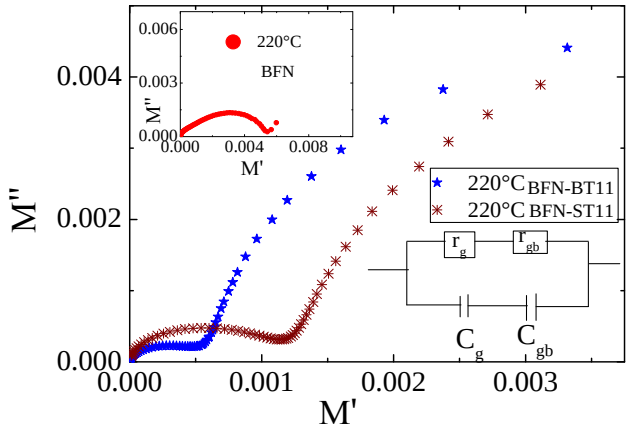

Fig. 9. Complex plane plot (M″ vs. M') of BFN, BFN-BT11 and BFN-ST11, ceramics, at 220°C and RC equivalent circuit (inset).

The complex modulus spectrum (M′ versus M″) of BFN, BFN-BT11 and BFN-ST11 ceramics at 220°C is shown in **Fig. 9**. For a bulk crystal containing interfacial boundary layer (grain-boundary), the equivalent circuit may be considered as two parallel RC elements connected in series (inset of **Fig. 9**.) and gives rise to two arcs in complex plane, one for bulk crystal (grain) and the other for the interfacial boundary (grain-boundary) response. The relative position of the two arcs in a complex modulus plane can be identified by the frequency. The arc of bulk generally lies on the frequency range higher than that of interfacial boundary since the relaxation time $\tau_m = \frac{1}{\omega_m}$ for the interfacial boundary is much larger than that for the bulk crystal.

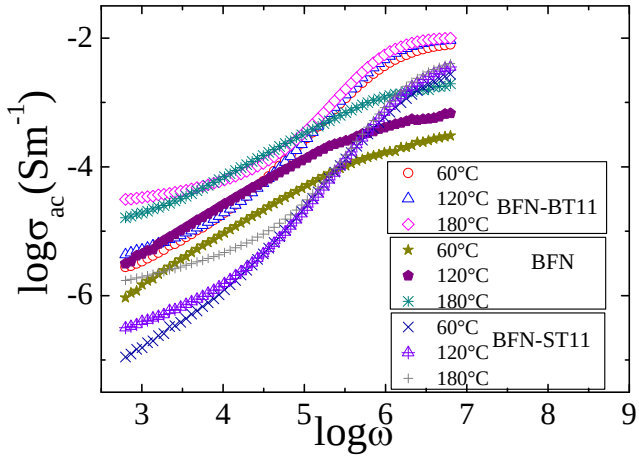

Fig. 10. Logarithmic angular frequency dependence of ac conductivity (σ_{ac}) for BFN, BFN-BT11 and BFN-ST11, ceramics at selected temperatures.

Conductivity formalism

It is to be noted that the high values of dielectric constant (ε′) and tangent loss (tanδ) in lower frequency region do not generally correspond to bulk effect. The high values of ε′ interestingly observed only at very high temperature and very low frequencies may be attributed to the fact that the free charges buildup at interfaces with in the bulk of the sample(interfacial Maxwell–Wagner (MW) polarization) **[37]** and at the interface between the sample and the electrodes space- charge polarization **[38]**. In order to elucidate this point, the frequency dependent ac conductivity (σ_{ac}) at various temperatures of BFN, BFN-BT11 and BFN-ST11 ceramics is plotted in **Fig. 10**. The real part of ac conductivity is given by the relation

$$\sigma_{ac} = \omega \varepsilon_0 \varepsilon'' \quad (1)$$

The nature of variation of electrical conductivity with frequency at lower temperatures exhibits conductivity dispersion. The ac conductivity increases sharply with rise in frequency and temperature. This increased conductivity is due to the movement of thermal ions (generally hopping motion of ions) from one preferable site to other. As the temperature rises, the conductivity spectrum shows low frequency plateau followed by high-frequency dispersion. The high-frequency conductivity dispersion may be attributed to ac conductivity whereas the frequency independent plateau region of the conductivity pattern corresponds to the dc conductivity (σ_{dc}) of the material.

Conclusion

In this work, we reported, structural, dielectric and impedance properties of $Ba(Fe_{0.5}Nb_{0.5})O_3$ (BFN), $0.89Ba(Fe_{0.5}Nb_{0.5})O_3$-$0.11BaTiO_3$ (BFN-BT11) and $0.89Ba(Fe_{0.5}Nb_{0.5})O_3$-$0.11SrTiO_3$ (BFN-ST11) compounds, prepared by a high-temperature solid state reaction method. X-ray diffraction studies of the compound showed the formation of single-phase monoclinic crystal structure at room temperature. Surface morphology of the compounds was studied by Scanning electron microscope (SEM). The variation of relative dielectric permittivity (ε′) and tangent loss (tanδ) may be attributed to hopping of trapped charge carriers, which resulted in an extra dielectric response in addition to the dipole response. The electrical properties of the samples were investigated in a frequency range of 100 Hz - 1 MHz and temperature range of 30°C-350°C using complex impedance spectroscopic technique. The frequency-dependent electrical data are also analyzed in the framework of conductivity and impedance formalisms.

Acknowledgement

The authors are grateful to DRDO, for providing financial assistance for this research grant.

References

1. Viehland, D.; Jang, S. J.; Cross, L. E.; Wutting, M. *Phys. Rev. B* **1992,** *46*, 8003.
2. Cross, L.E. *Ferroelectrics* **1994**,*151*, 305.
3. Uchino, K. *Ferroelectrics* **1994**, 15, 321.
4. Badapanda, T.; Rout, S.K.; Cavalcante, L.S.; Sczancoski, J.C.; Panigrahi, S.; Sinha, T.P.; Longo, E. *Materials Chemistry and Physics* **2010**, *121* 147. **DOI:**10.1016/j.matchemphys.2010.01.008
5. Himanshu, A. K.; Choudhary, B.K.; Gupta, D.C.; Bandyopadhayay, S.K.; Sinha, T.P. *Physica B* **2010**, *405*, 1608. **DOI:**10.1016/j.physb.2009.12.051
6. Roulland, F.; Terras, R.; Allainmat, G.; Pollet, M.; Marinel, S. *J. Eur. Ceram.Soc.* **2004**, *24*, 1019.
7. Saha, S.; Sinha, T.P. *Phys. Rev. B* **2002**, *65*, 134103. **DOI:**10.1103/PhysRev.65.1341XX

8. Raevski, I. P.; Prosandeev, S. A.; Bogatin, A. S.; Malitskya M. A.; Jastrabik, L. *J. Appl. Phys*. **2003**, *93*, 4130. **DOI:**10.1063/1.1558205
9. Chung, C. Y.; Chung, Y. H.; Chen, G. J. *J. Appl. Phys.* **2004,** *96*, 6624. **DOI:**10.1063/1.1804243
10. Wang, Z.; Chen, X. M.; Ni, L.; Liu, Y.Y.; Liu, X. Q. *Appl. Phys. Lett.* **2007**, *90*, 102905. **DOI:** 10.1063/1.2711767
11. Singh, N. K.; Kumar, P.; Rai, R *Journal of Alloys and Compounds* **2011**, *509*, 2957. **DOI:**10.1016/j.jallcom.2010.11.168
12. Singh, N. K.; Kumar, P.; Sharma, A. K.; Choudhary, R. N. P. *Materials Sciences and Applications*, **2011**, *2*, 1593. **DOI:**10.4236/msa.2011.211213
13. Intatha, U.; Eitssayeam, S.; Wang, J.; Tunkasiri, T. *Curr. Appl. Phys.* **2010**, *10*, 21. **DOI:**10.1016/j.cap.2009.04.006
14. Fang, B.; Cheng, Z.; Sun, R.; Ding, C.; *J. Alloys Compd.* **2009**, *47*, 539. **DOI:**10.1016/j.jallcom.2008.04.056
15. Nedelcu, L.; Toacsan, M. I.; Banciu, M.G.; Ioachim, A.; *J. Alloys Compd.* **2011**, *509*, 477. **DOI:**10.1016/j.jallcom.2010.09.069
16. Prasad, K.; Bhagat, S.; Amarnath, K.; Choudhary, S. N. ; Yadav, K. L. *Phys. Status Solidi A* **2009**, *206*.
17. Prasad, K.; Bhagat, S.; Amarnath, K.; Choudhary, S. N.; Yadav, K. L. *Mater. Sci Poland* **2010**, *28*.
18. Dutta, A.; Sinha, T. P. J. *Phys. Chem. Solids* **2006**, *67*, 1484.
19. Prasad, K.; Chandra, K. P.; Bhagat, S.; Choudhary, S. N. ; Kulkarni, A. R. *J. Amer.Ceram. Soc.* **2010**, *93*.
20. Singh, N. K.; Kumar, P.; Rai, R. *Adv. Mat. Lett.* **2011**, *2(3)*, 200. **DOI:** 10.5185/amlett.2010.11178
21. Manezok, R.; Wernicke, R. *Philips Tech. Rev*. **1983**, *41*, 338.
22. Burn, I.; Electrocomponent Sci. Technol. **1976**, *2*, 341.
23. Babbitt, R.W.; Koscica, T.E.; Drach, W.E. *J. Microwave*, **1992**, *35*, 63.
24. Heartling, G.H.; Land, C.E.; *Ferroelectric*s **1972,** *3*, 269.
25. Wul, E.; PowdMult, An interactive powder diffraction data interpretation and index program, version 2.1, school of Physical science, Flinders University of South Australia, Bedford Park, S.A. 5042, Australia.
26. Hench, L.L.; West, J.K. *Principles of Electronic Ceramics (Wiley, New York)* **1990**,189.
27. Singh, N. K.; Kumar, P.; Kumar, H.; Rai, R. *Adv. Mat. Lett.* **2010**, *1*, 79. **DOI:** 10.5185/amlett.2010.3102
28. Singh, N. K.; Kumar, P.; Roy, O. P.; Rai, R. *J. Alloys and Compounds* **2010**, *507*, 542. **DOI:** 10.1016/j.jallcom.2010.08.015
29. Kumar, P.; Singh, B. P.; Sinha,T. P.; Singh, N. K. *Physica B* **2011**, *406*, 139. **DOI:**10.1016/j.physb.2010.09.019
30. Kumar, P.; Singh, B. P.; Sinha,T. P.; Singh, N. K. *Adv. Mat. Lett.* **2011,** *2(1)*, 76. **DOI:** 10.5185/amlett.2010.11176
31. Sharma, S.; Rai, R.; Hall, D.A.; Shackleton, J. *Adv. Mat. Lett.* **2012,** *3(2)*, 92. **DOI:** 10.5185/amlett.2011.6279
32. Verma, K.; Sharma, S.; Sharma, D. K.; Kumar, Raju.; Rai, R. *Adv. Mat. Lett.* **2012,** *3(1)*, 44. **DOI:** 10.5185/amlett.2011.5264
33. Barik, S.K.; Choudhary, R.N.P; Singh, A.K. *Adv. Mat. Lett.* **2011,** *2(6)*, 419. **DOI:** 10.5185/amlett.2011.2228
34. Shantha, K.; Varma, K.B.R. *Solid State Ion.* **1997**, *99*, 225.
35. Saha, S.; Sinha, T.P. *J. Phys. Chem. Solids* **2006**, *67*, 1484.
36. Macedo, P.B.; Moynihan, C.T.; Bose, R. *Phys. Chem. Glasses* **1972**, *13*, 171.
37. Kyritsis, A.; Pissis, P.; Grammatikakis, J.; J. *Polym. Sci. Polym. Phys.* **1995**, *33*, 1737.
38. Jonscher, A.K. Dielectric Relaxation in Solids, *Chelsea Dielectric Press, London*, **1983**.

